

# **FRACTURE MECHANICAL BEHAVIOR OF CONCRETE AND THE CONDITION OF THE FRACTURE SURFACES ON DIFFERENT SCALES**

Viktor Mechtcherine

*Technical University of Kaiserslautern, Kaiserslautern, Germany*

## **ABSTRACT**

The fracture mechanical properties, in particular uniaxial tensile strength  $f_t$ , Young's modulus  $E_0$  and fracture energy  $G_F$  as well as the shape of the stress-strain and the stress-deformation relations were investigated for high-strength and normal strength concrete. In order to analyze failure mechanisms of these concretes, the roughness and the fractal dimension of the entire fracture surfaces and of their components (fractured aggregate, cement paste and cement paste-aggregate interface) were calculated on the basis of the optical measurements on meso and micro level, respectively. These data showed a clear correlation with fracture properties of the concretes investigated.

## **1 INTRODUCTION**

In recent years comprehensive research of fracture surfaces provided a better understanding of the energy consumption due to cracking and herewith on the formation and propagation of cracks in cementitious materials (Mechtcherine et al. 1995, Mechtcherine 2000).

In this study the effects of the concrete strength and the curing conditions on the formation and propagation of cracks in concrete were investigated. First, a series of deformation controlled uniaxial tension tests with two different set-ups were performed for normal strength concrete (NSC) and high-strength concrete (HSC). From the test data the characteristics of the material response, i.e. uniaxial tensile strength  $f_t$ , Young's modulus  $E_0$  and fracture energy  $G_F$  were evaluated.

As the second step, the condition of the fracture surfaces was studied on two different scales. The entire fracture surfaces of the tested specimens were investigated using a relatively coarse measurement grid ("meso scale") in order to understand fracture mechanisms and to explain the effect of the parameters under investigation on the fracture energy  $G_F$  and on the shape of the stress-crack opening diagrams ( $\sigma$ - $w$  relations) derived from the tests on notched specimens. The components of the failure surfaces – fractured aggregate, cement paste and cement paste-aggregate interface – were investigated on microscopic scale to provide additional information about the local failure mechanisms in concrete. These data were correlated with the shape of the stress-strain curves ( $\sigma$ - $\varepsilon$  relations) obtained from the experiments on unnotched prisms.

## **2 FRACTURE MECHANICAL EXPERIMENTS**

The composition of the two types of concrete which were investigated is given in Table 1. In both mixtures ordinary Portland cement CEM I 32.5 R was used. As aggregate quartzite Rhine sand and gravel were applied. The mixture for the HSC had a silica fume content of 45 kg/m<sup>3</sup>. By adjusting the dosage of a sodium naphthalene sulfonate type super plasticizer the same nominal spread (43 – 47 cm) for the both types of concrete could be achieved. Their compressive strength obtained from the tests on cube specimens at an age of 28 days was 96 MPa and 44 MPa, respectively.

Dog-bone shaped prisms with a gauge length of 250 mm were chosen to determine the uniaxial tensile strength  $f_t$ , the tangent modulus of elasticity  $E_0$ , as well as the  $\sigma$ - $\varepsilon$  diagram for increasing stresses (see Fig. 1, left). Notched prisms were used to determine fracture energy  $G_F$  and the complete stress-deformation relation. Both types of specimens had the same effective cross-section 60 × 100 mm<sup>2</sup>. A

schematic view of the specimen geometries and typical stress-deformation relations are given in Figure 1 (right). Details may be found in (Mechtcherine 2000).

Table 1: Composition of the concretes

Concrete	w/c	Cement [kg/m <sup>3</sup> ]	Silica Fume [kg/m <sup>3</sup> ]	Aggregate 0-16 mm [kg/m <sup>3</sup> ]	Super Plasticizer [kg/m <sup>3</sup> ]	$f_{cc}^{cube}$ [MPa]
HSC	0.33	450	45	1721	21	96
NSC	0.6	318	-	1811	1	44

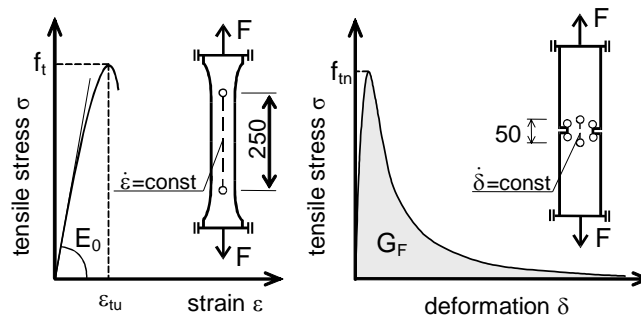


Figure 1: Schematic view of the geometry of dog-bone (left) and notched (right) specimens with typical stress-deformation relations (geometrical data in [mm])

All specimens were cast horizontally in metal forms. After demoulding, the specimens were wrapped in a thin plastic sheet to which an aluminum foil was glued in order to protect the concrete against desiccation. For the normal strength concrete under investigation also a parallel series of specimens were stored, after demoulding, unsealed in a climatic chamber at a relative humidity of 65 % and a temperature of 23 °C. All specimens were tested at an age of 56 days.

To assure a stable and possibly symmetrical crack propagation in the uniaxial tension tests, stiff metal plates were glued to the specimens. Finally, the metal plates were firmly connected with the bearing platens of the testing machine.

In the tests on the unnotched prisms the strain rate was controlled by means of the average signal of two LVDTs fixed to the specimens. In the experiments on the notched specimens four LVDTs with a gauge length of 25 mm were placed on the notch tips on both sides of the specimen to achieve a better deformation rate control. Two further LVDTs with a gauge length of 50 mm were placed in the middle of the notched cross-section to provide the data for the  $\sigma$ - $\delta$  relation (see Fig. 1, right). The tension tests on dog-bone shaped specimens were performed with a strain rate  $\dot{\epsilon}$  of  $10^{-6}$  1/s.

The corresponding deformation rate  $\dot{\delta}$  in the tension tests on notched specimens was  $5 \cdot 10^{-5}$  mm/s.

The ascending stress-strain relation for concrete subjected to uniaxial tension has a characteristic shape as shown in Figure 1 (left). While the relation is linear at low stresses the shape of the curve deviates from the linearity at higher stresses due to the microcrack formation, until it becomes horizontal at  $\sigma = f_t$ . A stable crack propagation could not be achieved with the particular test set-up used here.

According to Table 2, the tensile strength  $f_t$ , the tangent modulus of elasticity  $E_0$  and the strain  $\epsilon_{tu}$  (the strain at peak stress  $\sigma = f_t$ ) of the HSC are significantly higher than the corresponding values for the NSC. The unsealed normal strength concrete showed lower  $f_t$ - and  $E_0$ -values, and slightly lower values of the strain  $\epsilon_{tu}$  than the sealed NSC.

In the uniaxial tension tests on notched specimens also the descending branch of the  $\sigma$ - $\varepsilon$  relation could be determined up to nearly complete separation of the specimens into two parts because of the localized crack due to the notches and the reduction of the gauge length for the control of deformation rate to 25 mm. The values of the net tensile strength  $f_{tn}$ , the fracture energy  $G_F$  and the characteristic length  $l_{ch}$  obtained from these experiments are listed in Table 2.

The net tensile strength  $f_{tn}$  shows a similar dependence on the concrete composition and the curing conditions as the tensile strength  $f_t$  measured on the dog-bone specimens; however  $f_{tn}$  is lower than  $f_t$ , indicating a notch sensitivity of the concretes.

Table 2: Results of the uniaxial tension tests

Concrete	$f_t$ [MPa]	$E_0$ [MPa]	$\varepsilon_{tu} [\cdot 10^{-3}]$	$f_{tn}$ [MPa]	$G_F$ [N/m]	$l_{ch}$ [m]
HSC	6.1 (0.2)	47700 (170)	0.151 (0.005)	5.4 (0.7)	162 (21)	0.21
NSC sealed	3.8 (0.4)	36320 (1540)	0.130 (0.009)	2.9 (0.3)	135 (21)	0.34
NSC unsealed	3.1 (0.2)	33060 (750)	0.128 (0.01)	2.7 (0.4)	167 (24)	0.57

Standard deviations are given in parentheses.

The fracture energy  $G_F$  is defined as the energy per unit area needed for complete separation of a specimen into two parts. This value corresponds to the area under the  $\sigma$ - $w$  relation. The fracture energy of the high-strength concrete is higher than the corresponding value of the sealed normal strength concrete, but slightly lower than the fracture energy of the unsealed normal strength concrete.

The characteristic length  $l_{ch}$  ( $l_{ch} = G_F \cdot E_0 / f_t^2$ ) decreases with increasing strength of concrete. The specimens made of the NSC and protected from desiccation showed a smaller characteristic length than those of the unsealed concrete. The higher  $l_{ch}$ -values indicate a more ductile behavior of concrete.

### 3 QUANTIFICATION OF THE CONDITION OF THE FRACTURE SURFACES

To study the effect of the concrete strength and the curing conditions on the crack propagation the fracture surfaces from the uniaxial tension test were measured using the projected fringes technique (see Fig. 2, left). Height differences of the surface induce a lateral displacement of the projected strip pattern. The incorporation of geometrical data of the optical configuration then allows the contour information to be detected from the phase shift of the surface strip pattern at each surface location (Mechtcherine 2000). The measurement at intervals of 0.16 mm gives  $375 \times 625$  mesh data for each failure surface.

To study the condition of the components of the fracture surfaces the confocal microscope technique was applied. In this study  $512 \times 512$  mesh data have been used for each monitored spot of  $0.64 \times 0.64$  mm<sup>2</sup>. Details may be found in (Mechtcherine 2000).

From the optical measurement data the roughness and the fractal dimension of the surfaces were determined in order to quantify the condition of the entire fracture surfaces as well as of their components.

The roughness  $R_S$  of the entire fractured surface was calculated as the surface area measured with 0.16 mm mesh size and divided by the projected area. The fractal dimension was defined by the grid scaling method (Mechtcherine et al. 1995).

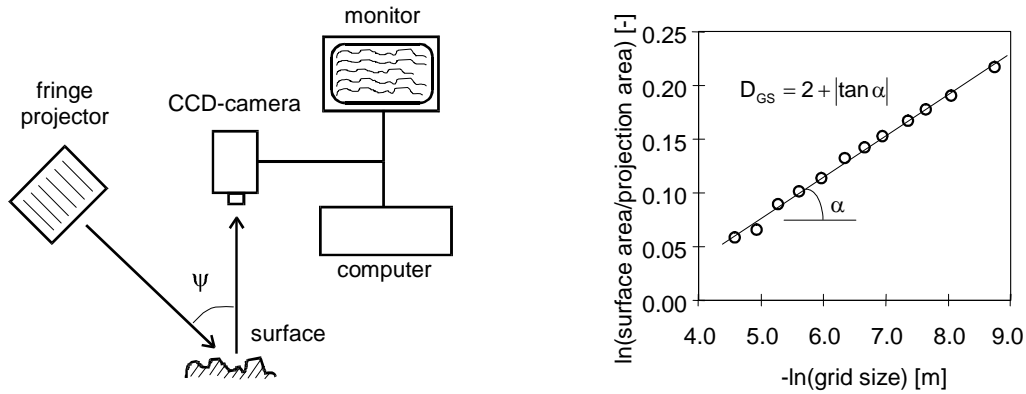


Figure 2: Principle of the projected fringes technique (left), and plot based on the grid scaling method applied to characterize the fracture surface of a typical concrete specimen (right)

This method is based on the fact that the measured surface area increases as the grid size decreases. The plot of the logarithm ( $\ln$ ) of the measured surface area (here related to projection area) over the logarithm of the grid size gives the negative value of fractal increment =  $\tan \alpha$  (Figure 2, right). The grid scaling fractal dimension  $D_{GS}$  can be calculated by adding this value to the dimension of a plane = 2. Table 3 gives the results of the calculations. The roughness and the fractal dimension of the fracture surface increase with decreasing strength of concrete. The fracture surfaces of the unsealed normal strength concrete are rougher than those of the sealed NSC.

Table 3: Roughness and fractal dimension of concrete fracture surfaces of the investigated concretes

Concrete	Roughness $R_S$	Fractal Dimension $D_{GS}$
HSC, sealed	1.167 (0.008)	2.029 (0.001)
NSC, sealed	1.258 (0.013)	2.044 (0.003)
NSC, unsealed	1.323 (0.040)	2.052 (0.003)

Standard deviations are given in parentheses.

Table 4: Roughness and fractal dimension of the fracture surfaces of the concrete components

Concrete	Components	Roughness $R_S$ [-]	Fractal Dimension $D_{GS}$ [-]
HSC, sealed	Cement paste	1.636 (0.239)	2.087 (0.027)
	Fract. aggregate	1.238 - 2.368	2.047 - 2.184
NSC, sealed	Cement paste	1.718 (0.047)	2.097 (0.016)
	CP/Agg.-Interface	1.465 (0.137)	2.080 (0.019)
NSC, unsealed	Cement paste	1.940 (0.159)	2.119 (0.011)
	CP/Agg.-Interface	1.782 (0.147)	2.111 (0.011)

Standard deviations are given in parentheses.

The roughness  $R_S$  of the components of fracture surfaces was derived from the surface area measured with 1.252  $\mu\text{m}$  mesh size. Also in this case the grid scaling method was applied to calculate the fractal dimension.

According to Table 4 the micro-roughness and fractal dimension of the fractured cement paste of the HSC are lower than the corresponding values of the NSC. The fractured cement paste of the unsealed NSC has the roughest surface. Also the cement paste-aggregate interface of the unsealed NSC is rougher than that of the sealed NSC. The fractured aggregates of the high-strength concrete provided rather strongly varying  $R_S$ - and  $D_{GS}$ -values. This was caused by a significant variation of the microstructure of the aggregated grains investigated.

#### 4 DISCUSSION OF THE EXPERIMENTAL RESULTS

With increasing strength of concrete an increase of the strain  $\varepsilon_{tu}$  was observed (Tab. 2 and Fig. 3, left). Drying of the normal strength concrete had no significant effect on this material parameter. However, considering only the non-linear deformation component of the strain  $\varepsilon_{tu,nl}$  ( $\varepsilon_{tu,nl} = \varepsilon_{tu} - f_t/E_0$ ) the highest values are obtained for the unsealed NSC and the lowest ones for the HSC. The  $\sigma$ - $\varepsilon$  relation of the NSC is more non-linear than that of the HSC due to the advanced micro-cracking which is observed for the NSC. Figure 3 (right) shows calculated non-linear strains  $\varepsilon_{nl}$  ( $\varepsilon_{nl} = \varepsilon - \sigma/E_0$ ), i.e. strains caused by micro-cracking. The unsealed NSC provided the most pronounced non-linearity.

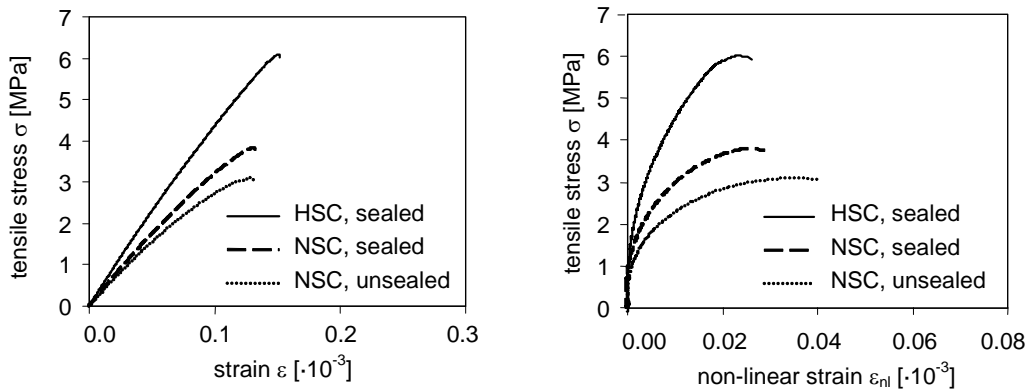


Figure 3: Measured  $\sigma$ - $\varepsilon$  relations (left) and calculated non-linear strains  $\varepsilon_{nl}$  at different stress levels (right) for the normal strength and the high-strength concretes

The non-linear strains, which represent a measure of the damage in concrete due to micro-cracking, correlate to the values of the roughness  $R_S$  and the fractal dimension  $D_{GS}$  detected for the components of the fracture concrete surfaces on the microlevel (refer to Tab. 4). It appears to be a consistent result that the pronounced micro-cracking for the NSC has to cause a rougher failure surface.

The uniaxial tension tests provided for the high-strength concrete approximately 20 % higher values of the fracture energy than the corresponding values of the sealed normal strength concrete. However, for the unsealed NSC a slightly higher  $G_F$ -value has been found than for the HSC.

Figure 4 shows the influence of the concrete strength and the curing conditions on the shape of the stress-deformation relation. For the HSC the area under the initial part of the  $\sigma$ - $\delta$  relation is larger than that for the NSC, because of a higher tensile strength and higher values for  $\delta_{tu}$ . This indicates an increase of energy consumption for the formation and propagation of narrow cracks with increasing strength of concrete. For larger crack widths this trend reverses, and the  $\sigma$ - $\delta$  relations for the NSC are above those for the HSC. This difference is small in the case of the sealed NSC, but it is significant in the case of the

unsealed NSC. The condition of the fracture surfaces gives an explanation for this phenomenon: the higher roughness and the higher fractal dimensions of the fracture surfaces of the NSC, especially of the unsealed ones (see Tab. 3) indicate a pronounced crack surface interlocking, which provides a better transfer of the tensile stresses across the crack.

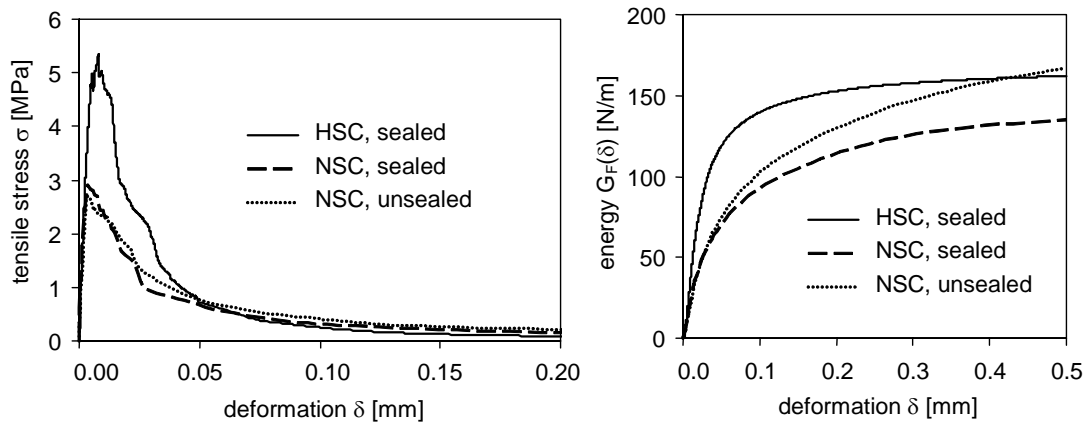


Figure 4: Influence of the concrete strength and the curing conditions on the shape of the  $\sigma$ - $\delta$  relation (left) and on the energy consumption due to the fracture process (right)

## 5 SUMMARY AND CONCLUSIONS

The investigated high-strength concrete has a higher strain  $\varepsilon_{tu}$  at tensile strength  $f_t$ , and when approaching the tensile strength, it has a lower value of the non-linear strain  $\varepsilon_{tu,nl}$  than a normal strength concrete. The strongest non-linearity of the  $\sigma$ - $\varepsilon$  relation, indicating the most advanced micro-cracking, was observed for the unsealed normal strength concrete. These observations correlate well with the results from the optical measurements of the micro-roughness of the fracture surfaces: the high-strength concrete provided the lowest and the unsealed normal strength concrete the highest values of the micro-roughness  $R_S$  and the fractal dimension  $D_{GS}$  on the microlevel.

The higher roughness  $R_S$  and the higher fractal dimension  $D_{GS}$  of the entire fracture surfaces of the NSC, especially of the unsealed one, indicate a better transfer of tensile stress across the crack. This results in a less steep descending branch of the  $\sigma$ - $\varepsilon$  relation and in higher energy consumption at larger crack widths in comparison to the high-strength concrete.

## 6 REFERENCES

- Mechtcherine, V., Garrecht, H., Hilsdorf, H. K.: Effect of temperature and loading rate on fracture behaviour of concrete subjected to uniaxial tension. *Fracture Mechanics of Concrete Structures*, F. H. Wittmann (ed.), Aedificatio Publishers, pp. 719-728, 1995.
- Mechtcherine, V.: Investigations on crack spreading in concrete. Doctoral thesis, University of Karlsruhe, in German, 2000.